PCCP

PAPER

View Article Online
View Journal | View Issue

Cite this: *Phys. Chem. Chem. Phys.*, 2016, **18**, 9537

Anisotropic Li intercalation in a Li_xFePO_4 nano-particle: a spectral smoothed boundary phase-field model

L. Hong,*† L. Liang, S. Bhattacharyya, W. Xing and L. Q. Chen

Received 13th January 2016,
Accepted 7th March 2016

DOI: 10.1039/c6cp00267f

www.rsc.org/pccp

A spectral smoothed boundary phase-field model is implemented to study lithium (Li) intercalation in a Li_xFePO_4 nano-particle immersed in a Li^+ rich electrolyte. It takes into account different physical processes on the particle surface, such as heterogeneous nucleation, Li flux and stress-free boundary conditions. We show the nucleation and growth of plate-like Li-rich crystallites along the (010) plane due to the high Li mobility along [001]. Since such plate-like crystallites, which are nucleated from (001) surfaces, align their phase boundaries along the (101) habit planes, a Li_xFePO_4 nano-particle with prominent (010) and (001) surface facets and the longest axis length along [100] is proposed to exhibit great mechanical stability.

1. Introduction

Olivine-structured Li_xFePO_4 is a promising cathode material for rechargeable Li-ion batteries, in which the Li intercalation process determines the mechanical stability and charging/discharging performances. Although there have been debates whether Li intercalation in Li_xFePO_4 takes places *via* a single-phase solid solution[1] or the formation of a two-phase mixture depending on the discharging rate, there is ample experimental evidence showing the coexistence of Li-rich and Li-lean phases[2–6] (denoted as LFP and FP, respectively). For example, phase diagrams of Li_xFePO_4, generated by the data from experiments[7] or theoretical calculations,[8,9] illustrate the two-phase mixture at room temperature. Since there is a large lattice mismatch between LFP and FP, the coherent strain energy is expected to play an important role in the intercalation process.

As it is challenging to detect *in situ* phase boundary movement of active Li-ion batteries, various intercalation mechanisms in single particles have been proposed, such as the shrinking core–shell model,[2] the wedge-like model,[4] the domino-cascade model[5] and the staging structure model.[10] However, these models are limited in revealing the elastic effects on the two-phase interfaces.[11,12] Although atomic computations[1] presented an alternative single-phase solid solution transformation path between FP and LFP phases to explain the remarkable rate capability of Li_xFePO_4, the *ab initio* simulations are restricted to a few material unit cells and often at zero temperature. On the other hand, mesoscopic continuum approaches parametrize the computational models, which have a similar size to the Li_xFePO_4 nano-particle, using *ab initio* bulk and surface properties, and have provided key understandings on the phase transition kinetics in Li_xFePO_4 at room temperature. Singh *et al.*[13] developed a general continuum theory to reveal the "traveling-wave" like movement of the phase boundary in Li_xFePO_4. Bai *et al.*[14] pointed out that the high discharging speed depressed phase separation. Nevertheless, elastic strain energy is ignored. Recently, a phase-field approach capable of modelling the effect of strain energy on microstructure evolution[15–17] has been applied to study the Li intercalation mechanism in Li_xFePO_4. For example, Cogswell and Bazant[12] incorporated elastic energy into their phase-field model to show the spinodal decomposition and the domain size dependence on the particle size. But, the surface traction free boundary condition and the surface facet dependent heterogeneous nucleation of the free standing Li_xFePO_4 nano-particle are not well constructed. Tang *et al.*[18] showed that the phase boundary is kinetically affected by the coherent strain energy during the Li charging/discharging process, providing an important interpretation to the *ex situ* observations.[3,4] One question is how to extend these models to execute the computation intensive tasks of examining the Li intercalation process in the porous electrode, which is composed of additives and multi-active-particles with arbitrary shapes. To realize it, we need a computational model that is efficient and capable of describing interfacial reactions and tracking multiphase and multicomponent transport at different length or timescales.

One promising way is to combine the spectral method[19] and the smoothed boundary approach.[20,21] The latter approach excels in describing physics-based multiphase and multicomponent transport phenomena, and implementing interfacial conditions on arbitrary interfaces. In the present work, we carry out the

Department of Materials Science and Engineering, The Pennsylvania State University, University Park, PA 16802, USA

† Present address: Department of Materials Science and Nanoengineering, Rice University, 6100 Main Street, Houston, TX 77005, USA. E-mail: lh26@rice.edu

spectral smoothed boundary phase-field model to investigate the Li intercalation kinetics in a Li_xFePO_4 nano-particle immersed in a Li^+ rich electrolyte. The detailed implementation, including derivations of heterogeneous nucleation, interfacial reaction and surface traction free conditions, is summarized in the Appendix for the future extension to the porous electrode. Although Li diffuses fast along [010] channels[22,23] in Li_xFePO_4 particles, which typically have prominent (010) surface facets,[24,25] these diffusion channels can be impeded by antisite defects.[26] Recently, Li ion transport in single crystal $LiFePO_4$ showed comparable mobilities along the three directions.[27] Moreover, [100]-oriented $LiFePO_4$ nanostructures are reported to have excellent electrochemical performance.[28] Thus, investigating the effects of coherent strain energy and Li diffusion along [100] and [001] directions on the nucleation behaviors and the Li intercalation process is necessary. In the present study, a two-dimensional (2D) phase-field model is used to study the Li intercalation process on the (010) plane.

2. Model

The FP and LFP phases are distinguished by the Li concentration $c(\vec{r})$ inside the Li_xFePO_4 nano-particle. The total free energy is expressed as

$$F_{\text{tot}} = \iiint_V \left[f_{\text{chem}}(c,T) + f_{\text{elas}}(\varepsilon_{ij},c) + \frac{\kappa}{2}(\nabla c)^2 \right] \mathrm{d}V, \qquad (1)$$

where the chemical energy density is expressed with regular solution formulation, $f_{\text{chem}}(c,T) = N_v[\Omega c(1-c) + k_B T(c\ln c + (1-c)\ln(1-c))]$, in which N_v is the number of atoms per unit volume of $FePO_4$, Ω is the regular solution parameter, k_B is the Boltzmann constant, and T is the temperature. We assume that the electron is delocalized with Li diffusion in Li_xFePO_4 nano-particles, thus the electron contribution to the polaron entropy is ignored in this study. Such an assumption has been adopted in most continuum models for the study of Li intercalation kinetics in Li_xFePO_4,[12,18] because the coupling relationship between the electron and Li in cathode Li_xFePO_4 is not well understood. The elastic energy density is $f_{\text{elas}}(\varepsilon_{ij},c) = \frac{1}{2}C_{ijkl}(\varepsilon_{ij} - \varepsilon^0_{ij}(c))(\varepsilon_{kl} - \varepsilon^0_{kl}(c))$, where the elastic stiffness C_{ijkl} is assumed to be concentration independent inside the particle. $\varepsilon^0_{ij}(c)$ is the eigenstrain induced by the misfit strain of two phases, and its value depends on local Li concentration. Assuming Vegard's law, $\varepsilon^0_{ij}(c) = \Delta e^0_{ij}(c - c_0)$, where Δe^0_{ij} is the misfit strain between LFP and FP, and c_0 is the Li concentration of FP. The total strain $\varepsilon_{ij} = \bar{\varepsilon}_{ij} + \eta_{ij}$ is composed of homogeneous strain $\bar{\varepsilon}_{ij}$ and heterogeneous strain η_{ij}. $\bar{\varepsilon}_{ij} = s_{ijkl}\left[\frac{1}{V}\int_V C_{klmn}\varepsilon^0_{mn}\mathrm{d}V\right]$ in the present free standing Li_xFePO_4 nano-particle. s_{ijkl} is the elastic compliance tensor and η_{ij} is obtained through the mechanical equilibrium. Note that this elastic model is reduced to 2D in the present study by assuming the plane strain condition.[12] The gradient energy density in eqn (1) is $f_{\text{gra}}(\nabla c) = \frac{\kappa}{2}(\nabla c)^2$, where κ is the gradient coefficient. In this paper, the Einstein summation convention is employed.

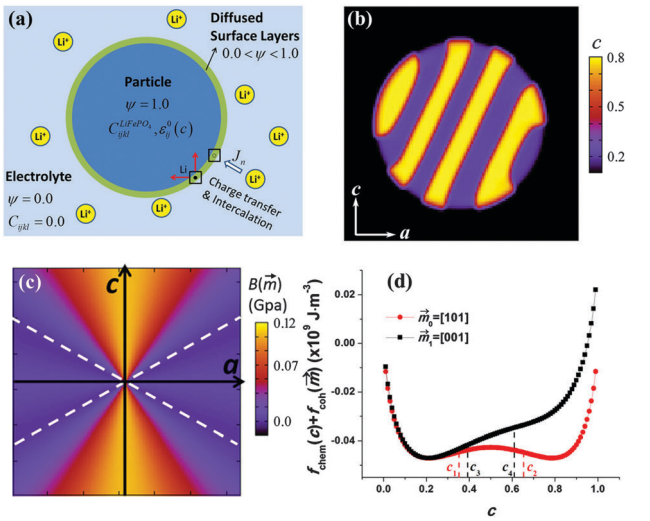

Fig. 1 (a) Schematic of the present computational model in which a Li_xFePO_4 nano-particle is surrounded by the Li^+ rich electrolyte. Domain parameter ψ separates the model into three parts, *i.e.*, Li_xFePO_4 particle, electrolyte and particle surface. (b) (101) phase boundaries after spinodal decomposition of FP (blue color) and LFP (yellow color) phases, which represent the Li-lean and Li-rich two phases, starting from an initial state of $c(\vec{r})$ = 0.5 with random noise perturbations. The phase boundary orientations are calculated through conversion from cubic to orthorhombic coordinate systems (Appendix D). The electrolyte medium is depicted in black color. (c) Variations of $B(\vec{m})$ on the *ac* plane as a function of $\vec{m}$ on the *ac* plane. The two dotted white lines indicate ⟨101⟩, the direction of the habit plane with minimum coherent strain energy. (d) Shrinking miscibility gap on (001) interfaces. The spinodal decomposition of (101) and (001) interfaces occurs within c_1–c_2 (0.35–0.65) and c_3–c_4 (0.39–0.61), respectively.

On the Li_xFePO_4 nano-particle surface, different boundary conditions that affect the nucleation and intercalation processes are implemented through the smoothed boundary method, in which a domain parameter ψ is defined to separate the present electrode/electrolyte model into three parts (Fig. 1a), *i.e.*, Li_xFePO_4 nano-particle (ψ = 1), electrolyte medium (ψ = 0) and particle surface ($0 < \psi < 1$). The Cahn–Hilliard equation in the form of the smoothed boundary approach[21] is utilized to describe the Li intercalation process (see Appendix A),

$$\frac{\partial c}{\partial t} = \frac{1}{\psi}\nabla\cdot\left[\psi\mathbf{M}\nabla\left(\frac{\partial f_{\text{chem}}}{\partial c} + \frac{\partial f_{\text{elas}}}{\partial c} - \frac{\kappa}{\psi}\nabla\cdot(\psi\nabla c) + \frac{\kappa}{\psi}\nabla\psi\cdot\nabla c\right)\right] + \frac{|\nabla\psi|}{\psi}J_n, \qquad (2)$$

where $\mathbf{M}$ is the Li mobility tensor in which only the diagonal components M^0_a and M^0_c are taken into consideration for the present 2D study, and the mobility is assumed to be independent of Li concentration. The expression of Li flux on the particle surface, *i.e.*, J_n, is

$$J_n = \rho_s(c,\vec{n},\mathbf{M})J^0_n = \left[\beta\frac{\nabla\psi}{|\nabla\psi|}\cdot\frac{\mathbf{M}}{M_{\text{ref}}}\right]J^0_n, \qquad (3)$$

where $\vec{n} = \frac{\nabla\psi}{|\nabla\psi|}$ is the unit of the inward normal vector locating on the particle surface. ρ_s is the effective intercalation sites per unit area, which depends on local Li concentration, surface orientation and Li

mobility. M_{ref} is equal to the maximum element of **M**. β, the Li activity coefficient of the surface activated state, is set to be $\left(1-\frac{c}{c_{max}}\right)$ to account for the excluded volume at the reaction site,[13,14] where c_{max} is the Li concentration of LFP. J_n^0 can be determined by the charge-transfer reactions through the Butler–Volmer equation.[14,18,29] Since this study aims to explore the anisotropic Li intercalation inside the particle, we assign a constant value to J_n^0 for simplicity.

In the present model, a 2D circular olivine nano-particle without a preferred surface facet is constructed by assuming isotropic surface energy. The heterogeneous nucleation behavior is related to the term $\frac{\kappa}{\psi}\nabla\psi\cdot\nabla c=\kappa|\nabla\log\psi|(\vec{n}\cdot\nabla c)$ in eqn (2) (see Appendix B). Here $\vec{n}\cdot\nabla c=\sqrt{\frac{2\Delta f}{\kappa}}\cos\theta$,[30,31] where Δf is the energy difference between $f_{chem}(c)$ and the minimum bulk energy, and θ is the rotation angle between the FP/LFP phase boundary and the particle surface orientation. The particle surface is stress-free, and the mechanical equilibrium is assumed at any time moment since the diffusion process is much slower than the mechanical relaxation, *i.e.*, $[\psi C_{ijkl}(\varepsilon_{kl}-\varepsilon_{kl}^0)]_{,j}=0$ (see Appendix C). Here we use the iterative-perturbation approach[32] to solve the mechanical equilibrium equation in this elastically inhomogeneous model, and use the semi-implicit spectral method[19] to speed up the simulations.

The simulation box of this cathode-electrolyte model is discretized as $128\Delta x\times 128\Delta y$. To describe a circular Li_xFePO_4 particle, we set $\psi=0.5+0.5\left(\tanh\frac{r_0-r}{\varsigma}\right)$, where $r_0=40\Delta x$, $\varsigma=2\Delta x$, and r measures the displacement of any grid to the particle center. The grid spacing in real space is set as $\Delta x/l_0=\Delta y/l_0=1.0$. We assume l_0 = 2.0 nm, which defines the FP/LFP interface width of about 6.0 nm, consistent with the experimental observation.[4] The gradient coefficient is $\kappa=5.6\times10^{-12}$ J cm^{-1}, close to the values used in other studies.[12,18] The other parameters are, *i.e.*, $N_v=8.396\times10^{28}$ m^{-3}, Ω = 59 meV,[33] T = 300 K, $\Delta e_{11}^0=0.0592$, $\Delta e_{33}^0=-0.0128$, C_{1111} = 138.9 GPa, C_{2222} = 198.0 GPa, C_{3333} = 173.0 GPa, C_{1122} = 72.8 GPa, C_{1133} = 52.5 GPa, C_{2233} = 45.8 GPa, C_{2323} = 36.8 GPa, C_{1313} = 50.6 GPa, and C_{1212} = 47.6 GPa.[34,35] $\Delta e_{22}^0=0$ in the plane strain condition. The above thermodynamic parameters determine Li concentration in FP as $c_0=0.2$.[33] The heterogeneous nucleation is controlled by setting $\theta=\frac{\pi}{2}$ because we neglect the surface energy variation to the Li concentration, yielding a 90° contact angle between FP/LFP phase boundaries and the particle surface (Fig. 1b). The mathematical derivation is shown in Appendix B. Note that, although the present continuum approach is able to describe the mesoscopic phase transition kinetics, one limitation is the neglect of the actual atomic structure on the interface.

3. Results

3.1 Isotropic intercalation

Fig. 2 shows phase morphologies of the Li intercalation process without elastic energy. There is no preferred interface orientation along both the circular (Fig. 2a) and oval (Fig. 2b) phase boundaries, which are generated by the isotropic and anisotropic mobility, respectively. The movement of FP/LFP phase boundaries follows the shrinking core–shell mechanism.[2,13] In this study, we select the dimensionless value of Li flux normal to the particle surface, $J_n^{0*}=0.02$, to finish the simulations within a reasonable time and maintain numerical stability, for both the isotropic (Fig. 2) and anisotropic (Fig. 3) Li intercalation processes. Moreover, M_a^{0*} and M_c^{0*} give the dimensionless value of Li mobility along the *a*-axis and the *c*-axis, respectively. Therefore, isotropic mobility means $M_a^{0*}=M_c^{0*}$, while anisotropic mobility has unequal M_a^{0*} and M_c^{0*}.

3.2 Anisotropic intercalation

Coherent strain energy determines the orientation of the phase boundary between FP and LFP. Firstly, we describe the elastic energy of a coherent plate-like inclusion within an infinite body of a cubic solid solution using continuous theory,[36,37] *i.e.*, $f_{coh}(c,\vec{m})=\frac{1}{2}B(\vec{m})(c-c_0)^2$, where $B(\vec{m})=C_{ijkl}\Delta e_{ij}^0\Delta e_{kl}^0-\vec{m}_i\sigma_{ij}^0\Omega_{jl}(\vec{m})\sigma_{lm}^0\vec{m}_m$, $\vec{m}$ is the normal direction of the interface, ${\Omega_{ij}}^{-1}=C_{iklj}\vec{m}_k\vec{m}_l$, and $\sigma_{ij}^0=C_{ijkl}\Delta e_{kl}^0$. The minimum of $B(\vec{m})$ yields the stable coherent phase boundary thermodynamically, which is also called a habit plane and $\vec{m}_0$ represents its normal direction, *e.g.*, $\min[B(\vec{m})]=B(\vec{m}_0)$. Variations of $B(\vec{m})$ as a function of $\vec{m}$ on the *ac* plane are shown in Fig. 1c. To compare with the continuous theory of strain energy, we conduct a spinodal decomposition simulation starting from an initial state of $c(\vec{r})=0.5$ with random noise perturbations, producing the same stable FP/LFP phase boundaries (Fig. 1b) as shown in Fig. 1c. This demonstrates the consistency of the continuous theory and our computational model. Note that Li_xFePO_4 possesses orthorhombic unit cells, while our computational cells are cubic, therefore converting habit planes from cubic to orthorhombic coordinates in order to compare experimental results directly is necessary. After such conversion (see Appendix D), the (101) habit planes can be distinguished in Fig. 1b and c. This habit plane is consistent with the experimental observations.[11] Additionally, kinetic effects on phase transitions are revealed through studying influences of different coherent FP/LFP interfaces on free energy. Fig. 1d shows the shrinking miscibility gap on (001) interfaces, which have the largest $B(\vec{m})$ value of the *ac* plane. This can be understood through the definition of the spinodal region, *i.e.*, $\frac{\partial^2[f_{chem}(c,T)+f_{coh}(c,\vec{m})]}{\partial c^2}<0$, and the positive coherent

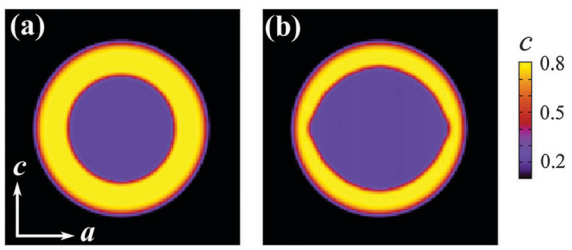

Fig. 2 Snapshots of the FP and LFP phase morphology during the Li intercalation process without elastic energy, for the cases with (a) isotropic mobility $M_a^{0*}=1.0$ and $M_c^{0*}=1.0$ and (b) anisotropic mobility $M_a^{0*}=0.0$ and $M_c^{0*}=1.0$.

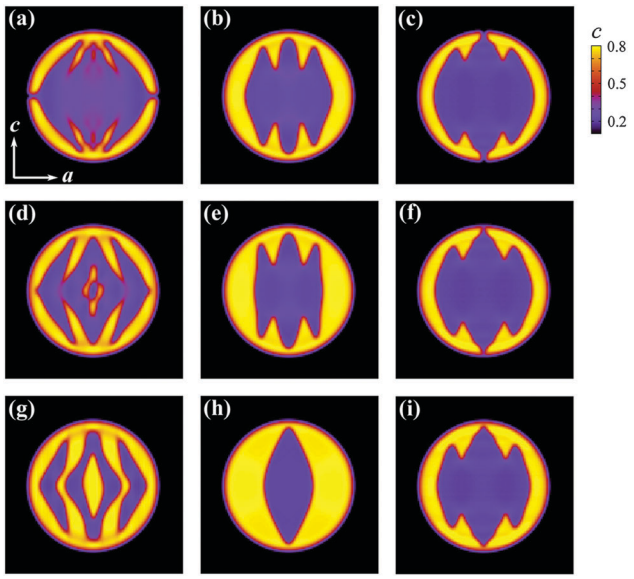

Fig. 3 Anisotropic Li intercalation process under the influence of elastic energy with anisotropic or isotropic Li mobilities. The three columns from left to right have the mobility $M_a^{0*} = 0.0$ and $M_c^{0*} = 1.0$, $M_a^{0*} = 1.0$ and $M_c^{0*} = 1.0$, $M_a^{0*} = 1.0$ and $M_c^{0*} = 0.0$, respectively. Snapshots of the FP and LFP phase morphology are shown in the sequence of simulation steps (a–c) 2.5×10^5, (d–f) 4×10^5 and (g–i) 7×10^5.

strain energy, *e.g.*, $B(\vec{m}) > 0$. From the above thermodynamic and kinetic analysis of coherent strain energy on phase transition behaviors, we find that the Li intercalation process in Li_xFePO_4 should be anisotropic, and thus strongly depends on Li diffusion mobilities along different axes.

Fig. 3 presents nucleation and Li intercalation kinetics with coherent strain energy under anisotropic or isotropic Li mobility, *i.e.*, $M_a^{0*} = 0.0$ and $M_c^{0*} = 1.0$ for Fig. 3a, d and g, $M_a^{0*} = 1.0$ and $M_c^{0*} = 1.0$ for Fig. 3b, e and h, and $M_a^{0*} = 1.0$ and $M_c^{0*} = 0.0$ for Fig. 3c, f and i. The initial nano-particle has single FP phase and the intercalation undergoes the same Li flux of the isotropic intercalation part. LFP starts the intercalation travelling wave from the particle shell, the same to the observation in ref. 4. Plate-like LFP is nucleated around the (001) surface of the particle for all simulations with isotropic or anisotropic mobility (Fig. 3a–c). These plate-like crystallites with (101) phase boundaries can penetrate and then swipe the cathode particle once the Li mobility along the *c*-axis is sufficiently larger than the one along the *a*-axis (Fig. 3g). The other two branches of the plate crystallites (Fig. 3a) merge together to produce LFP crystallites in the particle core. Such anisotropic intercalation accompanied by the production of separate LFP away from the particle surface is induced by the depressed spinodal decomposition on (001) interfaces (as shown in Fig. 1d) and the strongly anisotropic mobility (Fig. 3a, d and g). Therefore, the above anisotropic intercalation is one possible reason for the experimentally observed separation[38] of the lithiated core and the shell. On the other hand, the increase of Li mobility along the *a*-axis pins the growth of plate-like crystallite around the (001) surface, and promotes the movement of phase boundaries along the *a*-axis (Fig. 3b, e and h), which are nucleated around the (100) surface. If the Li diffusion along the *a*-axis dominates, the intercalation process is inhibited (Fig. 3c, f and i).

4. Discussion

The two-phase mixture in the Li_xFePO_4 nano-particle limits the charge and discharge rate owing to the low mobility of the phase boundary. This limitation can be diminished *via* single-phase solid solution transformation by increasing the coherency strain energy.[12] However, the high strain energy is more likely to induce cracks, which are commonly observed in Li_xFePO_4 particles[3,39] and act as an important degradation mechanism of the electrodes.[40,41] Recently, some schemes to tune electrochemical performances and mechanical stability of cathode Li_xFePO_4 have been proposed by utilizing Li transport along directions other than [010].[28,42] Under these conditions, the significant coherent strain energy stored in Li_xFePO_4 nano-particles is prone to be relaxed through destabilizing the metastable solid solution phase into the two-phase mixture. Therefore, more understandings on phase nucleation and coherent phase boundary propagation inside the nano-particles are needed.

This study shows that the significant variations of volume coherent strain energy among different phase boundaries have a remarkable effect on the heterogeneous LFP nucleation (Fig. 3), inducing plate-like LFP nucleation around the (001) surface facet of the Li_xFePO_4 nano-particle and uniform nucleation around the (100) surface. We also notice that the nucleated plate-like LFP nucleus grows and largely maintains their phase boundaries along the habit planes during the Li intercalation process with the strongly anisotropic mobility along [001]. A reduction in coherent strain energy during the Li charging/discharging processes beneficially reduces the overpotential required to initiate the phase transition between FP and LFP, and decreases the risks of generating cracks and dislocations.[43] Therefore, promoting nucleation and growth of plate-like lithiated phases, which strongly depends on the (001) surface area and the Li mobility along the *c*-axis, is a promising solution to reduce the energy consumption, prolong the battery life, and increase charging/discharging speed. Welland *et al.*[44] also proposed to engineer better battery performance *via* tuning surface wetting, but did not stress the significance of Li mobility along [001] and (001) surface areas. The complete wetting condition on the Li_xFePO_4 nano-particle[45] based on

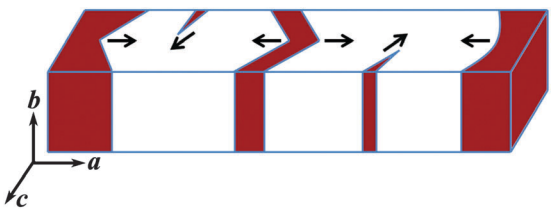

Fig. 4 Schematic of the proposed Li_xFePO_4 nano-particle with intercalated plate-like LFP crystallites (dark red). This particle has the major (010) and (001) surface facets, and a long length along the *a*-axis. The black arrows depict the growth directions of LFP crystallites.

thin interface approximation[12] may not be true in the cases with significant Li mobility along [001]. Based on the above discussion, a Li_xFePO_4 nano-particle (as shown in Fig. 4) with large (010) and (001) surface facets and the longest length along the *a*-axis has the greatest potential to efficiently enhance the discharging speed and maintains the mechanical stability during the electrochemical cycling reactions. This crystallite dimension shares some similarities to the one proposed by Van der Ven,[43] in which (100) phase boundaries show the lowest elastic energy.

5. Conclusions

The Li intercalation process under the influence of coherent strain energy is studied by employing a phase-field model, in which the shape of a cathode Li_xFePO_4 nano-particle is taken into consideration through the spectral smoothed boundary method. In contrast to the traditional shrinking core–shell mechanism without a preferred phase boundary orientation, the Li intercalation process is anisotropic if the coherent strain energy or anisotropic mobility is considered. The intercalated LFP with curved FP/LFP phase boundaries grows continuously from the shell to the core. A large diffusivity along [001] favors plate-like LFP phase regions. Since these crystallites maintain their phase boundaries along the habit planes, promoting the growth of plate-like LFP crystallites through the increase of Li mobility along [001] and the increase of (001) surface facets is beneficial to the mechanical stability of the Li_xFePO_4 nano-particles.

Appendix

A. The Cahn–Hilliard equation in the form of the smoothed boundary approach

The Cahn–Hilliard equation describing the phase transformation in bulk Li_xFePO_4 is expressed as

$$\frac{\partial c}{\partial t} = \nabla \cdot \mathbf{M}\nabla\left(\frac{\partial f_{\text{chem}}}{\partial c} + \frac{\partial f_{\text{elas}}}{\partial c} - \kappa\nabla\cdot\nabla c\right). \tag{A.1}$$

Multiplying domain parameter ψ to both sides of (A.1), we can obtain

$$\begin{aligned}\psi\frac{\partial c}{\partial t} &= \psi\nabla\cdot\mathbf{M}\nabla\left(\frac{\partial f_{\text{chem}}}{\partial c} + \frac{\partial f_{\text{elas}}}{\partial c} - \kappa\nabla\cdot\nabla c\right)\\ &= \nabla\cdot\psi\mathbf{M}\nabla\left(\frac{\partial f_{\text{chem}}}{\partial c} + \frac{\partial f_{\text{elas}}}{\partial c} - \kappa\nabla\cdot\nabla c\right)\\ &\quad - \nabla\psi\cdot\mathbf{M}\nabla\left(\frac{\partial f_{\text{chem}}}{\partial c} + \frac{\partial f_{\text{elas}}}{\partial c} - \kappa\nabla\cdot\nabla c\right)\\ &= \nabla\cdot\psi\mathbf{M}\nabla\left(\frac{\partial f_{\text{chem}}}{\partial c} + \frac{\partial f_{\text{elas}}}{\partial c} - \kappa\nabla\cdot\nabla c\right) + \nabla\psi\cdot\vec{J}_{\text{Li}},\end{aligned} \tag{A.2}$$

where Li flux $\vec{J}_{\text{Li}} = -\mathbf{M}\nabla\left(\frac{\partial f_{\text{chem}}}{\partial c} + \frac{\partial f_{\text{elas}}}{\partial c} - \kappa\nabla\cdot\nabla c\right)$. Thus,

$$\begin{aligned}\frac{\partial c}{\partial t} &= \frac{1}{\psi}\nabla\cdot\psi\mathbf{M}\nabla\left(\frac{\partial f_{\text{chem}}}{\partial c} + \frac{\partial f_{\text{elas}}}{\partial c} - \kappa\nabla\cdot\nabla c\right) + \frac{\nabla\psi}{\psi}\cdot\vec{J}_{\text{Li}}\\ &= \frac{1}{\psi}\nabla\cdot\psi\mathbf{M}\nabla\left(\frac{\partial f_{\text{chem}}}{\partial c} + \frac{\partial f_{\text{elas}}}{\partial c} - \kappa\nabla\cdot\nabla c\right) + \frac{|\nabla\psi|}{\psi}\frac{\nabla\psi}{|\nabla\psi|}\cdot\vec{J}_{\text{Li}}\\ &= \frac{1}{\psi}\nabla\cdot\psi\mathbf{M}\nabla\left(\frac{\partial f_{\text{chem}}}{\partial c} + \frac{\partial f_{\text{elas}}}{\partial c} - \kappa\nabla\cdot\nabla c\right) + \frac{|\nabla\psi|}{\psi}\vec{n}\cdot\vec{J}_{\text{Li}}\\ &= \frac{1}{\psi}\nabla\cdot\psi\mathbf{M}\nabla\left(\frac{\partial f_{\text{chem}}}{\partial c} + \frac{\partial f_{\text{elas}}}{\partial c} - \kappa\nabla\cdot\nabla c\right) + \frac{|\nabla\psi|}{\psi}J_n,\end{aligned} \tag{A.3}$$

where $\vec{n} = \frac{\nabla\psi}{|\nabla\psi|}$ is the unit of the inward normal vector locating on the particle surface. In order to consider the heterogeneous nucleation behaviors on the particle surface, we rewrite the third term inside the parentheses on the right hand side of (A.3), *i.e.*,

$$\kappa\nabla\cdot\nabla c = \frac{\kappa}{\psi}\psi\nabla\cdot\nabla c = \frac{\kappa}{\psi}\nabla\cdot\psi\nabla c - \frac{\kappa}{\psi}\nabla\psi\cdot\nabla c. \tag{A.4}$$

Thereby, we obtain eqn (2) in the main text.

B. Relation used in the derivation of controlling heterogeneous nucleation behaviors

Integrating the equilibrium criterion of the phase-field model from the interface to the bulk phase in one-dimension, we can obtain

$$\int_c^{c_{\text{bulk}}}\left(\frac{\partial f(c)}{\partial c} - \kappa\nabla^2 c\right)\mathrm{d}c = \int_c^{c_{\text{bulk}}}\mathrm{d}\left\{f(c) - \frac{\kappa}{2}(\nabla c)^2\right\} = 0, \tag{B.1}$$

where c_{bulk} gives the Li concentration of bulk phase. Thus we have $f(c) - \frac{\kappa}{2}|\nabla c|^2 = \text{const}_1$, where const_1 is a constant value. In the phase-field model, c_{bulk} remains uniform in the bulk away from the interface, thus $|\nabla c| = 0$ in the bulk. Therefore, $\text{const}_1 = f(c_{\text{bulk}})$ and $|\nabla c| = \sqrt{2\frac{f(c) - f(c_{\text{bulk}})}{\kappa}}$.

To illustrate the way of controlling heterogeneous nucleation behaviors, we rewrite the total free energy of the nano-particle into two explicit terms, including the bulk free energy and surface energy.

$$F_{\text{tot}} = \oiint_S Z(c)\mathrm{d}S + \iiint_V\left[f(c) + \frac{\kappa}{2}(\nabla c)^2\right]\mathrm{d}V. \tag{B.2}$$

The extremum of the free energy during the phase transformation can be found by solving the Euler–Lagrange equations.

Thus, we have

$$\begin{aligned}\delta F_{\text{tot}} &= \iint\!\!\!\bigcirc_S \left[\frac{\partial Z(c)}{\partial c}\delta c\right] \mathrm{d}S + \iiint_V \left[\frac{\partial f(c)}{\partial c}\delta c + \frac{\kappa}{2}\frac{\partial(\nabla c)^2}{\partial \nabla c}\nabla \delta c\right] \mathrm{d}V \\ &= \iint\!\!\!\bigcirc_S \left[\frac{\partial Z(c)}{\partial c}\delta c\right] \mathrm{d}S \\ &\quad + \iiint_V \left[\frac{\partial f(c)}{\partial c}\delta c + \frac{\kappa}{2}\nabla\left(\frac{\partial(\nabla c)^2}{\partial \nabla c}\delta c\right) - \frac{\kappa}{2}\delta c \nabla\left(\frac{\partial(\nabla c)^2}{\partial \nabla c}\right)\right] \mathrm{d}V \\ &= \iint\!\!\!\bigcirc_S \left[\frac{\partial Z(c)}{\partial c} - \kappa \vec{n}\cdot\nabla c\right]\delta c \mathrm{d}S + \iiint_V \left[\frac{\partial f(c)}{\partial c} - \kappa \nabla\cdot\nabla c\right]\delta c \mathrm{d}V,\end{aligned} \tag{B.3}$$

where $Z(c)$ represents the surface energy as a function of c. Minimization of the total free energy $\delta F_{\text{tot}} = 0$ yields the boundary condition,

$$\left[\frac{\partial Z(c)}{\partial c} - \kappa \vec{n}\cdot\nabla c\right]\delta c = 0 \text{ on } S. \tag{B.4}$$

In the present study, the surface energy variation to c is neglected due to the limited experimental data, *e.g.*, $\dfrac{\partial Z(c)}{\partial c} = 0$. Therefore, it is appropriate to assume $\kappa\vec{n}\cdot\nabla c = \kappa\sqrt{2\dfrac{f(c)-f(c_{\text{bulk}})}{\kappa}}\cos\theta = 0$ to satisfy the boundary condition (B.4). Thus we set $\theta = \dfrac{\pi}{2}$.

C. Derivation of the mechanical equilibrium equation

Since the mechanical equilibrium is usually established much faster than the diffusion processes, we have the mechanical equilibrium equation $\sigma_{ij,j} = 0$, where $\sigma_{ij} = C_{ijkl}(\bar{\varepsilon}_{kl} + \eta_{kl} - \varepsilon^0_{kl})$ is the elastic stress. Multiplying ψ on both sides yields

$$\psi\sigma_{ij,j} = (\psi\sigma_{ij})_{,j} - \psi_{,j}\cdot\sigma_{ij} = 0. \tag{C.1}$$

To impose the stress free boundary condition, *i.e.*, $\psi_{,j}\cdot\sigma_{ij} = 0$, then we have

$$(\psi\sigma_{ij})_{,j} = \lfloor C_{ijkl}(\vec{r})(\bar{\varepsilon}_{kl} + \eta_{kl} - \varepsilon^0_{kl})\rfloor_{,j} = 0, \tag{C.2}$$

where $C_{ijkl}(\vec{r}) = \psi C_{ijkl}$.

D. Conversion from cubic to orthorhombic coordinates

To convert the unit vector components normal to the FP/LFP phase boundary in the cubic computational grid cells to those in the crystallographic orientations of the orthorhombic crystal, we use

$$\begin{aligned} n^0_1 &= \frac{n_1/a}{\sqrt{(n_1/a)^2+(n_2/b)^2+(n_3/c)^2}} \\ n^0_2 &= \frac{n_2/b}{\sqrt{(n_1/a)^2+(n_2/b)^2+(n_3/c)^2}} \\ n^0_3 &= \frac{n_3/c}{\sqrt{(n_1/a)^2+(n_2/b)^2+(n_3/c)^2}}, \end{aligned} \tag{D.1}$$

where a, b, and c are lattice parameters of FP,[32] n_1, n_2, and n_3 are the components of the unit vector normal to the interface using the cubic grid cells, and n^0_1, n^0_2, and n^0_3 are the corresponding components in the orthorhombic crystal system.

Acknowledgements

The authors are grateful for the financial support by NSF under CMMI-1235092 and DOE Basic Sciences under the CMCSN Program. The computer simulations were carried out on the LION clusters at the Pennsylvania State University.

References

1 R. Malik, F. Zhou and G. Ceder, *Nat. Mater.*, 2011, **10**, 587.
2 A. K. Padhi, K. S. Nanjundaswamy and J. B. Goodenough, *J. Electrochem. Soc.*, 1997, **144**, 1188.
3 G. Chen, X. Song and T. J. Richardson, *Electrochem. Solid-State Lett.*, 2006, **9**, A295.
4 L. Laffont, C. Delacourt, P. Gibot, M. Y. Wu, P. Kooyman, C. Masquelier and J. M. Tarascon, *Chem. Mater.*, 2006, **18**, 5520.
5 C. Delmas, M. Maccario, L. Croguennec, F. Le Gras and F. Weill, *Nat. Mater.*, 2008, **7**, 665.
6 J. L. Allen, T. R. Jow and J. Wolfenstine, *Chem. Mater.*, 2007, **19**, 2108.
7 J. L. Dodd, R. Yazami and B. Fultz, *Electrochem. Solid-State Lett.*, 2006, **9**, A151.
8 F. Zhou, T. Maxisch and G. Ceder, *Phys. Rev. Lett.*, 2006, **97**, 155704.
9 S. I. Nishimura, G. Kobayashi, K. Ohoyama, R. Kanno, M. Yashima and A. Yamada, *Nat. Mater.*, 2008, **7**, 707.
10 L. Suo, W. Han, X. Lu, L. Gu, Y. S. Hu, H. Li, D. Chen, L. Chen, S. Tsukimoto and Y. Ikuhara, *Phys. Chem. Chem. Phys.*, 2012, **14**, 5356.
11 C. V. Ramana, A. Mauger, F. Gendron, C. M. Julien and K. Zaghib, *J. Power Sources*, 2009, **187**, 555.
12 D. A. Cogswell and M. Z. Bazant, *ACS Nano*, 2012, **6**, 2215.
13 G. K. Singh, G. Ceder and M. Z. Bazant, *Electrochim. Acta*, 2008, **53**, 7599.
14 P. Bai, D. A. Cogswell and M. Z. Bazant, *Nano Lett.*, 2011, **11**, 4890.
15 L. Q. Chen, *Annu. Rev. Mater. Res.*, 2002, **32**, 113.
16 W. J. Boettinger, J. A. Warren, C. Beckermann and A. Karma, *Annu. Rev. Mater. Res.*, 2002, **32**, 163.
17 Y. Z. Wang and J. Li, *Acta Mater.*, 2010, **58**, 1212.
18 M. Tang, J. F. Belak and M. R. Dorr, *J. Phys. Chem. C*, 2011, **115**, 4922.
19 L. Q. Chen and J. Shen, *Comput. Phys. Commun.*, 1998, **108**, 147.
20 A. Bueno-Orovio, V. M. Perez-Garcia and F. H. Fenton, *SIAM J. Sci. Comput.*, 2006, **28**, 886.
21 H. C. Yu, H. Y. Chen and K. Thornton, *Modell. Simul. Mater. Sci. Eng.*, 2012, **20**, 075008.
22 D. Morgan, A. Van der Ven and G. Ceder, *Electrochem. Solid-State Lett.*, 2004, **7**, A30.

23 M. S. Islam, D. J. Driscoll, C. A. J. Fisher and P. R. Slater, *Chem. Mater.*, 2005, **17**, 5085.
24 L. Wang, F. Zhou, Y. S. Meng and G. Ceder, *Phys. Rev. B: Condens. Matter Mater. Phys.*, 2007, **76**, 165435.
25 C. A. J. Fisher and M. S. Islam, *J. Mater. Chem.*, 2008, **18**, 1209.
26 R. Malik, D. Burch, M. Bazant and G. Ceder, *Nano Lett.*, 2010, **10**, 4123.
27 R. Amin, J. Maier, P. Balaya, D. P. Chen and C. T. Lin, *Solid State Ionics*, 2008, **179**, 1683.
28 Z. Li, Z. Peng, H. Zhang, T. Hu, M. Hu, K. Zhu and X. Wang, *Nano Lett.*, 2016, **16**, 795.
29 Y. H. Kao, M. Tang, N. Meethong, J. Bai, W. C. Carter and Y. M. Chiang, *Chem. Mater.*, 2010, **22**, 5845.
30 L. Granasy, T. Pusztai, D. Saylor and J. A. Warren, *Phys. Rev. Lett.*, 2007, **98**, 035703.
31 J. A. Warren, T. Pusztai, L. Kornyei and L. Granasy, *Phys. Rev. B: Condens. Matter Mater. Phys.*, 2009, **79**, 014204.
32 S. Y. Hu and L. Q. Chen, *Acta Mater.*, 2001, **49**, 1879.
33 B. C. Han, A. Van der Ven, D. Morgan and G. Ceder, *Electrochim. Acta*, 2004, **49**, 4691.
34 T. Maxisch and G. Ceder, *Phys. Rev. B: Condens. Matter Mater. Phys.*, 2006, **73**, 174112.
35 R. Rousse, J. Rodriguez-Carvajal, S. Patoux and C. Masquelier, *Chem. Mater.*, 2003, **15**, 4082.
36 A. G. Khachaturyan, *Theory of Structural Transformations in Solids*, Dover Publications, Mineola, New York, 2008.
37 J. W. Cahn, *Acta Metall.*, 1961, **9**, 795.
38 U. Boesenberg, F. Meirer, Y. Liu, A. K Shukla, R. Dell'Anna, T. Tyliszczak, G. Chen, J. C. Andrews, T. J. Richardson, R. Kostecki and J. Cabana, *Chem. Mater.*, 2013, **25**, 1664.
39 Y. S. Yu, C. Kim, D. A. Shapiro, M. Farmand, D. Qian, T. Tyliszczak, A. L. D. Kilcoyne, R. Celestre, S. Marchesini, J. Joseph, P. Denes, T. Warwick, F. C. Strobridge, C. P. Grey, H. Padmore, Y. S. Meng, R. Kostecki and J. Cabana, *Nano Lett.*, 2015, **15**, 4282.
40 J. Christensen and J. Newman, *J. Electrochem. Soc.*, 2006, **153**, A1019.
41 R. Deshpande, M. Verbrugge, Y. T. Cheng, J. Wang and P. Liu, *J. Electrochem. Soc.*, 2012, **159**, A1730.
42 L. Wang, X. He, W. Sun, J. Wang, Y. Li and S. Fan, *Nano Lett.*, 2012, **12**, 5632.
43 A. Van der Ven, K. Garikipati, S. Kim and M. Wagemaker, *J. Electrochem. Soc.*, 2009, **156**, A949.
44 M. J. Welland, D. Karpeyev, D. T. O'Connor and O. Heinonen, *ACS Nano*, 2015, **9**, 9757.
45 D. A. Cogswell and M. Z. Bazant, *Nano Lett.*, 2013, **13**, 3036.